Capacitive contribution to Li-storage in TiO_2 (B) and TiO_2 (anatase)

Barbora Laskova [a,b], Marketa Zukalova [a], Arnost Zukal [a], Milan Bousa [a,b], Ladislav Kavan [a,b,*]
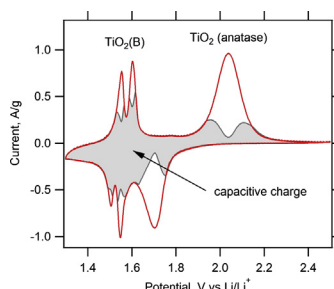
[a] J. Heyrovsky Institute of Physical Chemistry of the ASCR, v. v. i., Dolejskova 2155/3, CZ-182 23 Prague 8, Czech Republic
[b] Department of Inorganic Chemistry, Faculty of Science, Charles University, Hlavova 2030/8, CZ-128 43 Prague 2, Czech Republic

HIGHLIGHTS

- Capacitive parts of cyclic voltammograms of Li-storage were deconvoluted.
- TiO_2 (B) has by 30% larger capacitive contribution than anatase.
- The capacitive Li-storage in TiO_2 (B) occurs in bulk crystal.

GRAPHICAL ABSTRACT

ABSTRACT

Analysis of cyclic voltammograms of Li insertion into TiO_2 (B) and anatase provides information about capacitive contributions to overall charge of Li-storage. The enhancement of 30% is found in capacitive contributions (normalized to the total stored charges) in TiO_2 (B) compared to that in anatase, in spite of ca. three times smaller surface area of the former. Different charging mechanism explains facilitated Li^+ insertion in TiO_2 (B). The difference is caused mainly by pseudocapacitive Li-storage in the bulk TiO_2 (B). Deconvolution of cyclic voltammograms also indicates different capacitive contributions of the two voltammetric peaks, S1 and S2 of TiO_2 (B). These results provide novel insight into the Li-storage in TiO_2 (B) and its difference from that in anatase.

© 2013 Elsevier B.V. All rights reserved.

1. Introduction

TiO_2 (anatase) and TiO_2 (B) are attractive candidates for anodes in rechargeable Li-ion batteries, due to their low cost, non-toxicity, cycling stability at high charging rate, reasonable capacity and higher operating potential as compared to that of graphite anode [1–8]. The higher Li-insertion potential offers enhanced safety, and prevents formation of lithium dendrites in the battery, albeit at the expense of smaller energy density. The maximal Li-insertion coefficient x (in Li_xTiO_2) is usually close to 0.5 for anatase [9–11], but larger reversible capacities, $x \approx 0.8$ were also reported in certain anatase nanostructures [12–14]. Similar or even larger insertion coefficients were obtained for TiO_2 (B) [1–4,13–18]. The classical synthetic protocols for TiO_2 (B) [19–21] were modified to improve the capacity and charging rate [22–25]. TiO_2 (B) was prepared in the form of nanowires [22,23] ($x = 0.91$), nanoribbons ($x = 0.84$) [26], mesoporous TiO_2 (B) [27], nanoparticles and nanosheets ($x = 0.7–0.8$) [25,28].

* Corresponding author. J. Heyrovsky Institute of Physical Chemistry of the ASCR, v. v. i., Dolejskova 2155/3, CZ-182 23 Prague 8, Czech Republic. Tel.: +420 2 6605 3975; fax: +420 2 8659 2307.
E-mail address: kavan@jh-inst.cas.cz (L. Kavan).

TiO$_2$ (B) is metastable modification of titanium dioxide, adopting the monoclinic structure, space group $C2/m$, lattice parameters: $a = 12.127$ Å, $b = 3.7537$ Å, $c = 6.535$ Å, $\beta = 107.16°$ [29]. Zukalova et al. [21] found that Li-insertion into TiO$_2$ (B) is characterized by unusually large faradaic pseudocapacitance. This peculiar effect was ascribed to Li$^+$ accommodation in open channels of TiO$_2$ (B) structure allowing fast Li-transport in TiO$_2$ (B) lattice along the b-axis (perpendicular to (010) face). The presence of several lithium insertion sites inside the channels of the TiO$_2$ (B) structure was predicted by theoretical calculations, but significant contradictions remain about the relative accessibility of these sites [24,30–33]. Another peculiarity follows from the existence of two surface-like voltammetric peaks (S1 and S2, with formal potentials of 1.52 and 1.59 V, respectively [21]) in the cyclic voltammogram of TiO$_2$ (B), as theory predicts three different sites (labeled A1, A2 and C [7,18,24,28,30,31,34,35], or A, B, C [32]) in the TiO$_2$ (B) structure, where Li can be accommodated. Furthermore, the Li-insertion into the lowest-energy site might also be mismatched with anatase impurity in a sample [24,31]. Therefore deeper insight into charging mechanisms in TiO$_2$ (B) is still needed.

The charge equivalent of Li-ion storage in TiO$_2$ is superposition of diffusion-controlled Li-insertion in the bulk crystal and capacitive contribution of double-layer charging. The capacitive charging is important particularly for nanocrystalline TiO$_2$ materials, due to their large surface areas. Specific questions arise from the pseudocapacitive Li-storage in TiO$_2$ (B), which is assumed to occur in the bulk crystal [21]. Here we present a detailed voltammetric analysis of lithium insertion to compare the charging mechanisms of TiO$_2$ (B) and anatase. To this purpose, we adopted the method developed by Dunn et al. [36,37]. The overall stored charge was separated into the contribution from fast processes assigned to capacitive and/or pseudocapacitive ones, and contribution from diffusion-controlled Li-insertion into the bulk [11,36–38].

2. Experimental section

2.1. Materials

TiO$_2$ (B) was synthesized using a method previously reported by Zukalova et al. [21]. Briefly, 10 g of amorphous TiO$_2$ was mortared with 7.8 g of Cs$_2$CO$_3$ (Aldrich). This powder was then calcined at 800 °C for 4 h, mortared again, and heated to 800 °C in a crucible with a tight lid for 48 h to form cesium titanate. Excess of 1 M HCl was added to the solid and stirred vigorously for 4 × 24 h with the fresh acid exchanged every 24 h. The product was finally dried in air. To optimize the synthetic conditions for high crystallinity and phase purity of TiO$_2$ (B), this precursor was annealed stepwise in the temperature range 100–1000 °C on the Pt stage of X-ray diffractometer. The diffractogram was measured in situ immediately after each 100 °C step, and by the comparison of particular diffractograms with the JCPD diffraction pattern No. 35-0088, the optimum heat treatment conditions were found to be 500 °C for 1 h in air. The Brunauer–Emmett–Teller (BET) surface area of the product was $S_{BET} = 28$ m^2 g^{-1}. The material is further coded HTi19. For comparison was used a reference anatase sample coded C240 [10]. It is a nanocrystalline anatase with S_{BET} of 89 m^2 g^{-1}, prepared by hydrolysis of titanium tetra(isopropoxide) and hydrothermal recrystallization at 240 °C in autoclave [10,39]. The morphology of C240 is characterized by particles ca. 10–20 nm in size exposing mainly the (101) facets [40]. The titanium dioxide P90 (from Degussa AG, Germany) was a second reference material. This powder had a BET area of 90 m^2 g^{-1} (rutile/anatase mixture with >90% anatase, average anatase particle size 13 nm and very small amount of TiO$_2$ (B)) [41]. Another material for comparison (denoted N21) was a sample obtained from SusTech GmbH & Co. KG,

Darmstadt, Germany. Its synthesis was described elsewhere [42]. Briefly, 8 mL of TiCl$_4$ was dissolved in 20 mL of water and 10 M NaOH was added to a total volume of 150 mL. The mixture was autoclaved at 250 °C for 6 h. Subsequently, the material was washed with hydrochloric acid and water and further autoclaved in water or weak acidic solvents for up to several hours. The concentrations of TiO$_2$ (B) and anatase phases were determined from powder X-ray diffraction (XRD) according to a method developed by Zhang et al. [43]. The N21 powder contained 49% TiO$_2$ (B), 51% anatase and had surface area $S_{BET} = 43$ m^2 g^{-1} [42].

2.2. Preparation of electrodes

The powder samples were sonicated in ethanol. Titanium grid (5 × 25 mm^2, Goodfellow) was used as the electrode support. The electrodes were prepared by dip-coating and the coated area was 5 × 10 mm^2 leaving uncovered edge for electrical contact. The electrodes were dried in air and then sintered in air at 450 °C for 30 min. The final mass of active material on a grid was adjusted between 0.30 and 0.62 mg. Blank experiments with Ti-grids annealed at the same conditions proved a negligible electrochemical charge capacity of the Ti grid compared to that of the active material.

2.3. Methods

Electrochemical measurements were carried out in a one-compartment cell using Autolab Pgstat-30 (Ecochemie) controlled by the GPES-4 software. LiN(CF$_3$SO$_2$)$_2$ (Fluka) was dried at 130 °C/ 1 mPa. Ethylene carbonate (EC) and 1,2-dimethoxyethane (DME) were dried over the 3 Å molecular sieve (Fluka). The electrolyte solution was 1 M LiN(CF$_3$SO$_2$)$_2$ in EC + DME (1/1 v/v). The reference and counter electrodes were from Li metal, hence, all potentials were quoted against the Li/Li$^+$ reference electrode in this medium. All electrochemical measurements were carried out under argon atmosphere in a glove box. The BET surface areas of the prepared materials were determined from nitrogen adsorption isotherms at 77 K using the Micromeritics ASAP 2020 instrument. The X-ray diffraction (XRD) was investigated on powder sample by RIGAKU Multiflex diffractometer using CuKα radiation. Raman spectra were measured on Micro Raman (LabRAM HR, Horiba Jobin-Yvon) with 633 nm excitation. Microscope (Olympus BX, objective 50×) allowed focusing laser beam on different grains of the solid material to test the homogeneity of studied sample. Scanning electron microscopy (SEM) images were obtained using a Hitachi field-emission-scanning electron microscope S-4800.

3. Results and discussion

The powder X-ray diffraction pattern of the as-prepared TiO$_2$ (B) (sample HTi19) is shown in Fig. 1a. The diffractogram confirms the presence of TiO$_2$ (B), monoclinic metastable polymorph of TiO$_2$ (space group $C2/m$, JCPD No. 35-0088). The sample is free from anatase, which is the usual impurity in various TiO$_2$ (B) materials. However, the main diagnostic diffraction peaks of TiO$_2$ (B) and anatase overlap. This decreases the sensitivity of phase analysis by XRD, and alternative methods, such as Raman spectroscopy or Li-insertion electrochemistry, are needed to test the sample purity [21] (see below). Raman spectrum of HTi19 (Fig. 1b) shows vibrational features of pure TiO$_2$ (B) without any features of anatase [21,22,25,27–29,44–47]. The centrosymmetric ($C2/m$) structure of TiO$_2$ (B) with four formula units in the primitive cell corresponds to 18 Raman-active vibration modes, $12A_g + 6B_g$. A comparison of theoretically calculated [29] and our experimental spectrum allows tentative assignment, which is labeled in Fig. 1b. Scanning electron
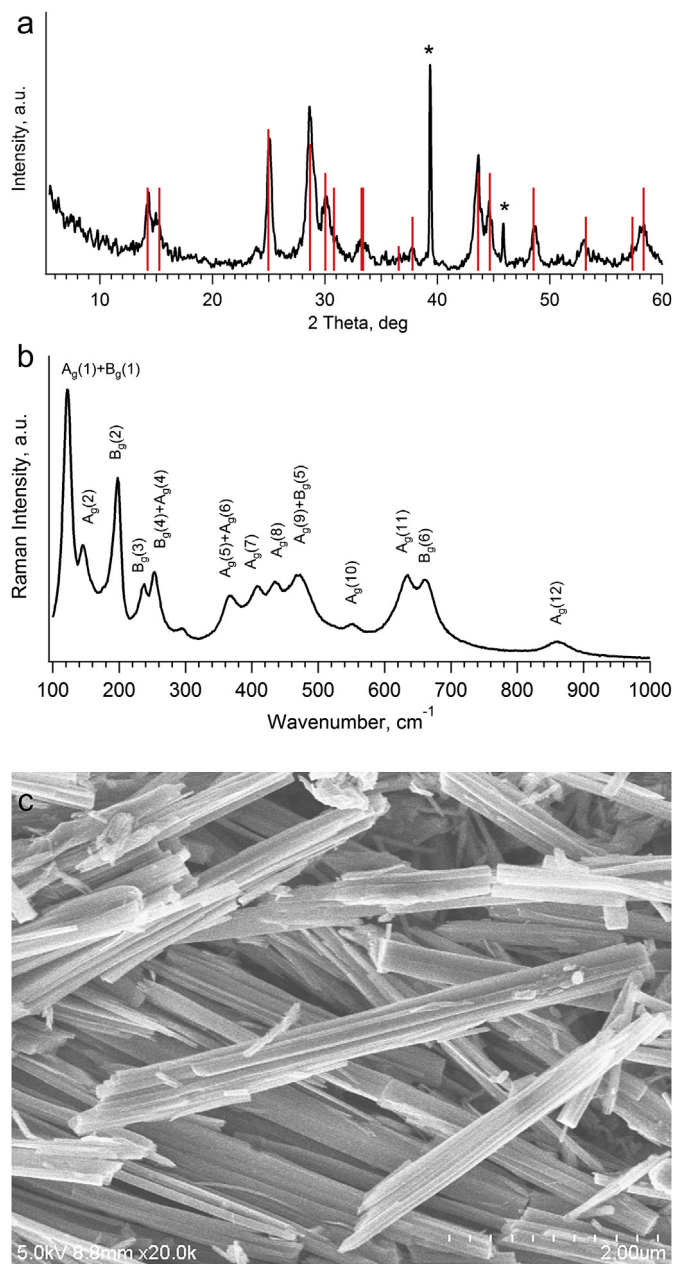
Fig. 1. The X-ray diffraction pattern (a), Raman spectrum (b) and SEM image (c) of HTi19 sample. The red lines in diffractogram (a) correspond to the diffraction pattern JCPD No. 35-0088. Diffraction peaks marked by asterisks arise from Pt sample stage. (For interpretation of the references to color in this figure legend, the reader is referred to the web version of this article.)

Fig. 2. Adsorption isotherms of nitrogen at 77 K of TiO_2 (B) (sample HTi19), anatase reference materials (samples C240, P90) and TiO_2 (B)/anatase composite (sample N21).

'surface-confined' nature of these peaks. It manifests itself by (i) very small (<59 mV) cathodic/anodic peak-to-peak splitting and (ii) the first-power dependence of peak current (i_p) on the scan rate (v), which is diagnostic for capacitive charging [7,8,18,21,50,51]. However, some authors also reported on the square-root dependence ($i_p \approx v^{1/2}$), indicating the diffusion-controlled charging in S1/S2 peaks [35] or both possibilities [27], and the solid-state Li-diffusion coefficients of the order of 10^{-14} to 10^{-16} cm^2 s^{-1} were calculated based on this assumption. To address these conflicting issues, cyclic voltammetry of the Li$^+$ insertion into HTi19 and into three reference materials (C240, P90, N21) was analyzed in detail according to the previously reported method [36–38]. The current response at a fixed potential can be expressed by:

$$i(V) = k_1 v + k_2 v^{1/2} \tag{1}$$

where $k_1 v$ corresponds to the capacitive current contribution associated with the storage of Li$^+$ at the TiO_2 surface and also to the bulk faradaic pseudocapacitance, specific for TiO_2 (B) [21]. The second term $k_2 v^{1/2}$ corresponds to the diffusion-controlled current, which is attributed to the insertion of Li$^+$ in the bulk of TiO_2 lattice. Dividing of equation (1) by $v^{1/2}$ leads to:

$$\frac{i(V)}{v^{1/2}} = k_1 v^{1/2} + k_2 \tag{2}$$

By linear fitting of measured voltammetric currents, at each specific potential, it is possible to determine the coefficients k_1 and k_2, and to distinguish between the contribution of capacitive current and diffusion-controlled current.

The electrodes from pure TiO_2 (B) (sample HTi19), anatase (C240, P90) and mixture of both phases (sample N21) were prepared with the same mass of the active material (0.58 ± 0.04 mg) to avoid any inaccuracy in CV data analysis due to different amount of active material on electrode. In addition to this series of experiments, the electrode with 0.3 mg of anatase C240 (coded C240half) was also prepared to test the influence of material mass on the computed capacitive contributions. The peak shift occurring as a result of different sweep rates was neglected and the cyclic

microscopy (SEM) image shown in Fig. 1c confirms fibrous texture, characteristic for TiO_2 (B) materials [21]. Adsorption isotherms of nitrogen at 77 K of the sample HTi19 and all three reference materials are presented in Fig. 2. The BET surface area of particular samples was calculated from the part of corresponding isotherm in the range of relative pressures 0.05–0.25.

Electrochemical properties were studied by cyclic voltammetry (CV) of Li-insertion. The absence of any features assignable to the Li insertion/extraction to/from anatase at ca. 1.7 V and 2.0 V, respectively (Fig. 3a) further confirms the phase purity of our HTi19 sample. The voltammogram of TiO_2 (B) exhibits two pairs of peaks labeled S1 and S2. This notation was introduced by us in Refs. [21,48,49] and adopted by others [7,8,50,51] to stress the
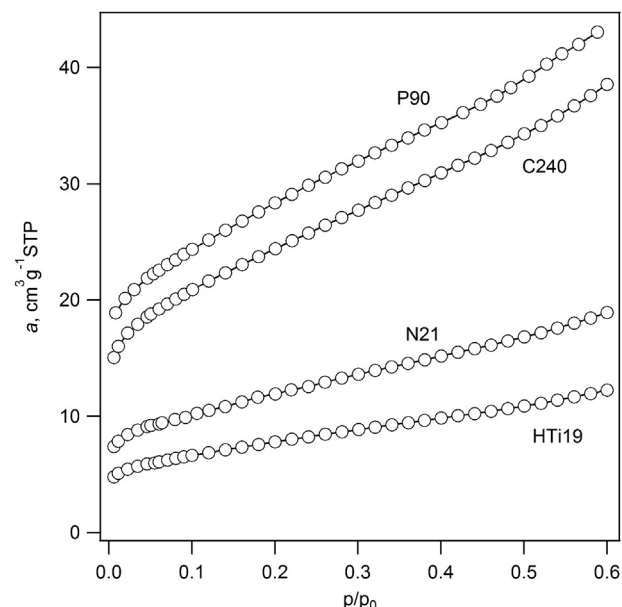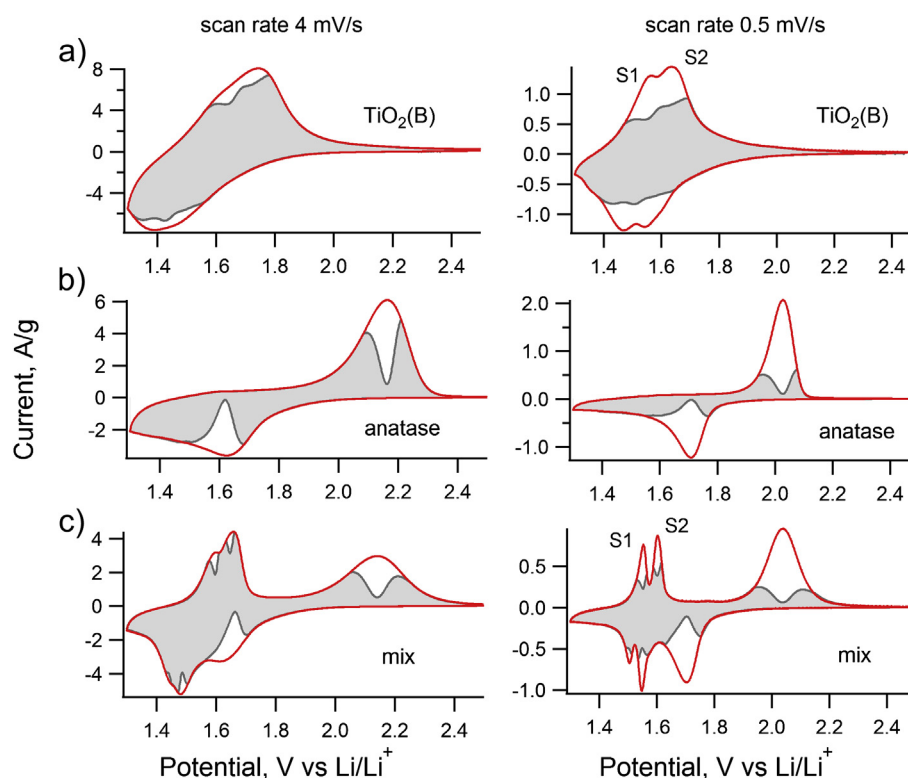
Fig. 3. The cyclic voltammograms of TiO$_2$ (B) (sample HTi19) (a), anatase (sample C240) (b) and mixture of both phases (sample N21) (c). The voltammograms are displayed for scan rates 4 mV s^{-1} (left charts) and 0.5 mV s^{-1} (right charts). The red lines correspond to experimentally obtained voltammetric currents. The shaded areas represent calculated capacitive contributions. S1 and S2 peaks in TiO$_2$ (B) are distinguished, particularly at slower scans (right charts a, c). (For interpretation of the references to color in this figure legend, the reader is referred to the web version of this article.)

voltammograms at 0.1 mV s^{-1} were used to define the potential of the current peak maximum [36]. The scan rates in a range of 4 mV s^{-1}–0.1 mV s^{-1} were chosen for analysis since the voltammetric peaks of all studied materials were well distinguishable at these rates. The voltammetric responses of electrodes HTi19, C240 and N21 at scan rates 4 mV s^{-1} and 0.5 mV s^{-1} are shown in Fig. 3 along with the calculated pseudocapacitive contributions to the total charges. Here, we adopted the convention introduced by Dunn et al. [36,37], i.e. the (pseudo)capacitive contribution is represented by shaded area in the voltammograms. To avoid any effect of data processing potential range, all measurements were made in the same way, and quantitative analysis of pseudocapacitive contributions was applied only in a specific range of potentials. To compare correctly all samples, the potential range was set as ±0.16 V from the maximum of the corresponding voltammetric peak. The majority of diffusion contribution (over 99%) occurred in this potential range. For extended potential ranges, only proportionally higher pseudocapacitive currents were observed for all the samples. Fig. 3 indicates that the (pseudo)capacitive charge is dominating in the voltammogram of TiO$_2$ (B) phase (Fig. 3a), and that of the TiO$_2$ (B) component in our mixed sample N21 (Fig. 3c) in comparison with that of anatase (sample C240, Fig. 3b).

The comparison of pure TiO$_2$ (B) and anatase electrodes is particularly interesting as the surface area of our TiO$_2$ (B) sample is only 28 m^2 g^{-1}, whereas the surface area of our anatase is 89 m^2 g^{-1}, i.e. larger by a factor of about 3. Our finding obviously contradicts the logical conclusion that the capacitive contribution is confined to the surface, i.e. it should scale with surface area (or reverse particle size) of TiO$_2$ [36]. For anatase electrodes, this was indeed confirmed: the found capacitive contributions were 55, 35, ad 15% for materials having the surface areas of 220, 150 and 50 m^2 g^{-1},

respectively (particles sizes of 7, 10 and 30 nm, respectively) [36]. Our comparison of TiO$_2$ (B) and anatase evidences that the capacitive Li-storage in TiO$_2$ (B) is qualitatively different and not confined to the surface only. This supports the idea of faradaic pseudocapacitance in the bulk crystal of TiO$_2$ (B) as proposed by Zukalova et al. [21].

The calculated contributions of capacitive charge to the overall accommodated Li for extraction peaks at different scan rates are shown in Table 1. The pseudocapacitive contribution for TiO$_2$ (B) (sample HTi19) is still high at the scan rate 0.5 mV s^{-1}. This contribution represents 68% of the total charge and matches well the result for the TiO$_2$ (B) peaks in the CV of mixed sample N21, which is 72%. The capacitive contributions for TiO$_2$ (B) are by about

Table 1
Comparison of capacitive charge storage contribution to the total stored charge for phase pure TiO$_2$ (B) material (HTi19); anatase reference samples (C240, P90); the anatase component in N21 (N21anatase) and the TiO$_2$ (B) component in N21 (N21TiO$_2$(B)). C240half denotes the results for anatase electrode with mass of active material of 0.3 mg. The individual charges Q^+_{cap}, Q^-_{cap}, Q^+_{diff}, Q^-_{diff} were determined for scan rate of 0.5 mV s^{-1}.

Scan rate		HTi19	C240	C240 half	P90	N21 anatase	N21TiO$_2$ (B)
4 mV s^{-1}	Capacitive contribution (%)	89	68	69	71	67	89
0.5 mV s^{-1}	Capacitive contribution (%)	68	37	38	41	38	72
	Q^+_{cap} (C g^{-1})	426	162	154	189	241[a]	
	Q^+_{diff} (C g^{-1})	199	273	249	273	211[a]	
	Q^-_{cap} (C g^{-1})	447	167	152	181	324[a]	
	Q^-_{diff} (C g^{-1})	177	260	215	265	133[a]	

[a] Total charge integrated for anatase and TiO$_2$ (B) components of the N21 sample.

30% higher than the same contributions for anatase (samples C240, P90) and the anatase peak in the voltammogram of N21 at 0.5 mV s^{-1}. These results agree with data evaluated for the C240 electrode with lower active mass. Hence, the 30% enhancement of capacitive contributions in TiO$_2$ (B) (referred to that in anatase) is independent on the amount of electrode material. It can be also deduced that the particle size of anatase crystals in material N21 is close to that in C240 and P90 samples because of their similar capacitive contributions [36].

For the given range of potentials the overall charge storage in pure anatase (C240 and P90) at scan rate 0.5 mV s^{-1} was 435 C g^{-1} and 462 C g^{-1} respectively. The total stored charge 625 C g^{-1} in pure TiO$_2$ (B) material (HTi19) was by ca. 27% higher than that in anatase. Considering the error of CV deconvolution to be ca. 10% [36], then the observed difference in overall charge storage is close to the calculated one for corresponding capacitive contributions. The voltammetric charges normalized to BET surface area equal 4.9 and 5.1 C m^{-2} for C240 and P90, respectively, but 22.3 C m^{-2} for pure TiO$_2$ (B), sample HTi19. These results indicate, that previously discussed fast Li$^+$ insertion into TiO$_2$ (B) and its higher Li insertion coefficient (x) [21,23,27,42,52] are caused by higher level of pseudocapacitive charge storage. Table 1 further compiles the actual anodic and cathodic charges (Q_{cap}^+ and Q_{cap}^-) corresponding to capacitive charge storage and analogous quantities for diffusion-controlled charge storage (Q_{diff}^+ and Q_{diff}^-) at the scan rate of 0.5 mV s^{-1}. Reasonably symmetrical charging/discharging is observed for both types of contributions in phase-pure samples, i.e. in HTi19, C240 and P90. The bi-modal sample, N21, does not allow accurate distinction of charges assignable to each individual phase, because of overlapping voltammetric features of TiO$_2$ (B) and anatase. Nevertheless the total voltammetric charge of N21 shows again good symmetry: $Q_{cap}^+ + Q_{diff}^+ = 452$ C g^{-1}; $Q_{cap}^- + Q_{diff}^- = 457$ C g^{-1}.

The lithium ion can be accommodated at three specific sites inside TiO$_2$ (B) structure labeled A1, A2 and C (using the more common coding, see above) [18,24,28,30−32,34,35]. The A1 and A2 sites are localized close to equatorial oxygen atoms of the TiO$_6$ octahedra and are both 5-fold coordinated; the C site is 4-fold co-ordinated by axial (bridge) oxygen atoms and sits near the middle of the open *b*-axis channel. From our results and these computations we suppose that there is a substantial pseudocapacitive process in TiO$_2$ (B) connected with accommodation of Li inside the TiO$_2$ (B) open channels and this process apparently causes the main difference in electrochemical response of TiO$_2$ (B) and anatase. This conclusion also supports earlier experimental works [21,27]. The capacitive contribution was reported by Dunn et al. [36,37] to be inversely proportional to a particle size of anatase. In our case, the anatase materials had particle size about 10−20 nm and BET surface area close to 90 m^2 g^{-1}. The TiO$_2$ (B) fibers had three times lower BET surface area ($S_{BET} = 28$ m^2 g^{-1}) and a length in the order of μm. In spite of their so large aspect ratio and difference in size, the TiO$_2$ (B) samples still have a significantly larger pseudocapacitive contribution to overall charge storage. This further highlights the influence of morphology and open channels in TiO$_2$ (B) structure on its improved electrochemical charge storage capacity.

The supposed overall deviation of contributions given by CV deconvolution process is up to 10% [36], nevertheless, the observed deviation of contributions was different for each potential and it was minimal at potential corresponding to the current peak ($<$1%). The contribution of Li$^+$ diffusion process has the highest value at the potential of current peak too and thus the most pronounced difference in the ratio of capacitive contributions to the total current can be expected at potentials of the current maxima for all the samples. Therefore the capacitive/diffusion contributions at potentials corresponding to the current maxima of extraction peaks of all the samples were investigated separately. Both types of

contributions at the current peak maxima for different scan rates were calculated by procedure described above.

Fig. 4 shows computed pseudocapacitive current ($k_1 \cdot v$) and diffusion-controlled current ($k_2 \cdot v^{1/2}$) as a function of the scan rate for the extraction peaks of HTi19 and C240. The current connected with Li$^+$ extraction from the bulk predominates over capacitive current for each scan rate more than five times in anatase (C240, Fig. 4a). On the other hand the pseudocapacitive current dominates to the total current until the scan rate of 0.5 mV s^{-1} for both peaks (S1 and S2 [21]) in CVs of HTi19 (see Fig. 4b and c). This high contribution of capacitive current at the potential of the peak maxima in HTi19 at slow scan rates clearly indicates the high pseudocapacitive storage in this material too [38]. The same conclusion follows from comparison of other anatase-containing materials, P90 and N21. The calculated contributions of the
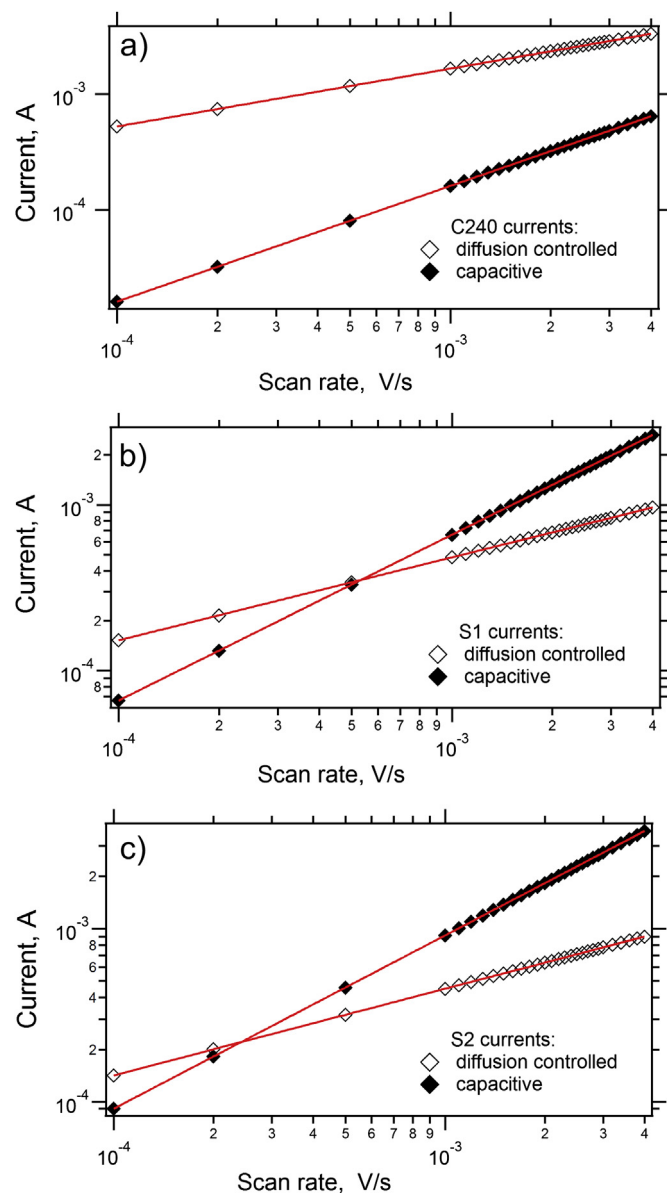

Fig. 4. Dependence of the calculated capacitive currents (full points) and diffusion controlled currents (open points) on scan rate for extraction peak maxima of anatase C240 (a), HTi19 peak at lower potentials S1 (b) and HTi19 peak at higher potentials S2 (c). The red lines represent fits corresponding to $k_1 v$ for capacitive processes and $k_2 v^{1/2}$ for diffusion processes, respectively. (For interpretation of the references to color in this figure legend, the reader is referred to the web version of this article.)

Table 2
Comparison of capacitive current contributions to the total current at peak maxima for phase pure TiO_2 (B) material (HTi19), the TiO_2 (B) component in N21 (N21TiO_2 (B)), the anatase reference samples (C240, P90) and the anatase component in N21 (N21anatase). C240half denotes the results for anatase electrode with mass of active material of 0.3 mg. The low-potential extraction peak of TiO_2 (B) is labeled as S1 and higher-potential extraction peak as S2.

	Scan rate	C240	C240half	P90	HTi19		N21TiO_2 (B)		N21anatase
					S1	S2	S1	S2	
Capacitive contribution (%)	4 mV s^{-1}	17	2	21	76	85	62	74	18
	0.5 mV s^{-1}	6	7	8	47	58	32	45	7

capacitive to the total current at the current peak maximum for different scan rates are summarized in Table 2. The data in Table 2 clearly show the capacitive contributions for TiO_2 (B) being of over 30% higher than those for anatase at 0.5 mV s^{-1}. Although there is a small difference in the actual data for pure TiO_2 (B) material HTi19 and the TiO_2 (B) component in N21, the high pseudocapacitive contribution as compared to that of anatase is still evident. For phase-pure sample (HTi19) and anatase samples is this difference even larger than 40%.

Theoretical studies of Li$^+$ accommodation sites in TiO_2 (B) and their stability were made recently [24,30–32,34]. However, they are contradictory as far as the preferential sites occupancy is concerned [24,31,32,34]. Arrouvel et al. [30] determined C site as the preferential one for Li$^+$ accommodation at $x < 0.25$, contrary to Dalton et al. [31], who concluded A1 site being more favorable for x lower than 0.5. Koudriachova [34], on the other hand, proposed that pseudocapacitive Li-storage is associated exclusively with the A2 site, but the effect of nanowire morphology also plays a role. Furthermore, the capacitive to overall contribution is lower for the low-potential extraction/insertion peak of TiO_2 (B) (denoted as S1 peak) in comparison with the higher-potential extraction/insertion peak (denoted as S2 peak), (see Figs. 4b, c, and Table 2). This effect is probably a result of saturation of the open b-axis channels by Li$^+$ at lower potentials. It can be assumed, that Li$^+$ is predominantly accommodated in certain sites at higher potentials and with potential decrease it diffuses from channels to the bulk material simultaneously. Since Li transport along the b-axis is faster than insertion into the bulk [30], the channels become almost saturated for potentials under 1.5 V and the decrease of pseudocapacitive contribution is observed for peak S1.

4. Conclusions

The charging mechanism of TiO_2 (B) and anatase during Li$^+$ insertion was investigated by deconvolution of cyclic voltammograms. The contribution of capacitive charge referred to the total stored charge was found to be over 30% higher in TiO_2 (B) compared to that in anatase nanocrystals, in spite of the factor of 3 smaller surface area of the former. The predominant pseudocapacitive process in TiO_2 (B) was related to accommodation of Li inside the TiO_2 (B) open channels in monoclinic lattice. The main difference in electrochemical response of TiO_2 (B) and anatase is caused by the pseudocapacitive processes in TiO_2 (B). To the best of our knowledge, this conclusion is here quantified for the first time. Moreover, the scan rate dependencies of cyclic voltammetry peak currents revealed different level of capacitive current for two voltammetric peaks (S1, S2) in TiO_2 (B). The capacitive contribution to the overall peak current was higher for voltammetric peak at higher potential (S2). This behavior is ascribed to saturation of open channels in the structure by Li$^+$ at lower potentials.

Acknowledgment

References

[1] Z. Yang, D. Choi, S. Kerisit, K.M. Rosso, D. Wang, J. Zhang, G. Graff, J. Liu, J. Power Sources 192 (2009) 588–598.
[2] P.G. Bruce, B. Scrosati, J.-M. Tarascon, Angew. Chem. Int. Ed. 47 (2008) 2930–2946.
[3] M. Wagemaker, F.M. Mulder, Acc. Chem. Res. 46 (2008) 1206–1215.
[4] S.T. Myung, N. Takahashi, S. Komaba, C.S. Yoon, Y.K. Sun, K. Amine, H. Yashiro, Adv. Funct. Mater. 21 (2011) 3231–3241.
[5] B.C. Melot, J.-M. Tarascon, Acc. Chem. Res. 46 (2012) 1226–1238.
[6] Z. Guo, X. Dong, D. Zhou, Y. Du, Y. Wang, Y. Xia, RSC Adv. 3 (2013) 3352–3358.
[7] C. Jiang, J. Zhang, J. Mater. Sci. Technol. 29 (2013) 97–122.
[8] S. Liu, H. Jia, L. Han, J. Wang, P. Gao, D. Xu, J. Yang, S. Che, Adv. Mater. 24 (2012) 3201–3204.
[9] S.Y. Huang, L. Kavan, M. Grätzel, I. Exnar, J. Electrochem. Soc. 142 (1995) L142–L144.
[10] L. Kavan, M. Grätzel, J. Rathousky, A. Zukal, J. Electrochem. Soc. 143 (1996) 394–400.
[11] H. Lindström, S. Södergen, A. Solbrand, H. Rensmo, J. Hjelm, A. Hagfeldt, S.E. Lindquist, J. Phys. Chem. B 101 (1997) 7717–7722.
[12] D. Bresser, E. Paillard, E. Binetti, S. Krueger, M. Striccoli, M. Winter, S. Passerini, J. Power Sources 206 (2012) 301–309.
[13] T. Berger, D. Monllor-Setoca, M. Jankulovska, T. Lana-Villarreal, R. Gomez, Chem. Phys. Chem. 13 (2012) 2824–2875.
[14] L. Kavan, Chem. Rec. 12 (2012) 131–142.
[15] B. Zachau-Christiansen, K. West, T. Jacobsen, S. Skaarup, Solid State Ionics 53–56 (1992) 364–369.
[16] B. Zachau-Christiansen, K. West, T. Jacobsen, S. Atlung, Solid State Ionics 28–30 (1988) 1176–1182.
[17] L. Brohan, R. Marchand, Solid State Ionics 9-10 (1983) 419–424.
[18] A.G. Dylla, G. Henkelman, K.J. Stevenson, Acc. Chem. Res. 46 (2013) 1104–1112.
[19] R. Marchand, L. Brohan, M. Tournoux, Mater. Res. Bull. 15 (1980) 1129–1133.
[20] T. Kasuga, M. Hiramatsu, A. Hoson, T. Sekino, K. Niihara, Langmuir 14 (1998) 3160–3163.
[21] M. Zukalova, M. Kalbac, L. Kavan, I. Exnar, M. Grätzel, Chem. Mater. 17 (2005) 1248–1255.
[22] A.R. Armstrong, G. Armstrong, J. Canales, P.G. Bruce, Angew. Chem. Int. Ed. 43 (2004) 2286–2288.
[23] A.R. Armstrong, G. Armstrong, J. Canales, P.G. Bruce, J. Power Sources 146 (2005) 501–506.
[24] A.R. Armstrong, C. Arrouvel, V. Gentili, S.C. Parker, M.S. Islam, P.G. Bruce, Chem. Mater. 22 (2010) 6426–6432.
[25] M. Kobayshi, V.V. Petrykin, M. Kakihana, Chem. Mater. 19 (2007) 5373–5376.
[26] T. Beuvier, M. Richard-Plouet, M. Mancini-Le Granvalet, T. Brousse, O. Crosnier, L. Brohan, Inorg. Chem. 49 (2010) 8457–8464.
[27] A.G. Dylla, J.A. Lee, K.J. Stevenson, Langmuir 28 (2012) 2897–2903.
[28] A.G. Dylla, P. Xiao, G. Henkelman, K.J. Stevenson, J. Phys. Chem. Lett. 3 (2012) 2015–2019.
[29] M.B. Yahia, F. Lemoigno, T. Beuvier, J.S. Filhol, M.R. Plouet, L. Brohan, M.L. Doublet, J. Chem. Phys. 130 (2009) 204501–20450111.
[30] C. Arrouvel, S.C. Parker, M.S. Islam, Chem. Mater. 21 (2009) 4778–4783.
[31] A.S. Dalton, A.A. Belak, A. Van der Ven, Chem. Mater. 24 (2012) 1568–1574.
[32] D. Panduwinata, J.D. Gale, J. Mater. Chem. 19 (2009) 3931–3940.
[33] T. Okumura, T. Fukutsuka, A. Yanagihara, Y. Orikasa, H. Arai, Z. Ogumi, Y. Uchimoto, Chem. Mater. 23 (2011) 3636–3644.
[34] M.V. Koudriachova, Surf. Interface Anal. 42 (2010) 1330–1332.
[35] C.W. Mason, I. Yeo, K. Saravanan, P. Balaya, RSC Adv. 3 (2013) 2935–2941.
[36] J. Wang, J. Polleux, J. Lim, B. Dunn, J. Phys. Chem. C 111 (2007) 14925–14931.
[37] T. Brezesinski, J. Wang, J. Polleux, B. Dunn, S.H. Tolbert, J. Am. Chem. Soc. 131 (2009) 1802–1809.
[38] K. Zhu, Q. Wang, J.H. Kim, A.A. Pesaran, A.J. Frank, J. Phys. Chem. C 116 (2012) 11895–11899.
[39] C. Barbe, F. Arendse, P. Comte, M. Jirousek, F. Lenzmann, V. Shklover, M. Grätzel, J. Am. Ceram. Soc. 80 (1997) 3157–3171.
[40] M. Grätzel, Prog. Photovolt. Res. Appl. 14 (2006) 429–442.
[41] L. Kavan, R. Bacsa, M. Tunckol, P. Serp, S.M. Zakeeruddin, F. Le Formal, M. Zukalova, M. Grätzel, J. Power Sources 195 (2010) 5360–5369.

[42] L. Kavan, M. Kalbac, M. Zukalova, I. Exnar, V. Lorenzen, R. Nesper, M. Grätzel, Chem. Mater. 16 (2004) 477–485.

[43] H. Zhang, M. Finnegan, J.F. Banfield, Nano Lett. 1 (2001) 81–85.

[44] T. Beuvier, M. Richard-Plouet, L. Brohan, J. Phys. Chem. C 113 (2009) 13703–13706.

[45] B. Santara, P.K. Giri, K. Imakita, M. Fujii, Nanoscale 5 (2013) 5476–5488.

[46] G. Xiang, Y.G. Wang, J. Li, J. Zhuang, X. Wang, Sci. Rep. 3 (2013) 1411–1411-6.

[47] W. Zhuang, L. Lu, X. Wu, W. Jin, M. Meng, Y. Zhu, X. Lu, Electrochem. Commun. 27 (2013) 124–127.

[48] L. Kavan, J. Rathousky, M. Grätzel, V. Shklover, A. Zukal, J. Phys. Chem. B 104 (2000) 12012–12020.

[49] L. Kavan, J. Rathousky, M. Grätzel, V. Shklover, A. Zukal, Micropor. Mesopor. Mater. 44-45 (2001) 653–659.

[50] J. Wang, Y. Zhou, Z. Shao, Electrochim. Acta 97 (2013) 386–392.

[51] H. Zhang, G.R. Li, L.P. An, T.Y. Yan, X.P. Gao, H.Y. Zhu, J. Phys. Chem. C 111 (2007) 6143–6148.

[52] M. Inaba, Y. Oba, F. Niina, Y. Murota, Y. Ogino, A. Tasaka, K. Hirota, \ 189 (2009) 580–584.